Received: 9 January 2018 | Accepted: 8 March 2018

DOI: 10.1111/jace.15538

Journal of the American Ceramic Society

INVITED FEATURE ARTICLE

First-principles study in an inter-granular glassy film model of silicon nitride

Wai-Yim Ching[1] | **Masato Yoshiya**[2,3] | **Puja Adhikari**[1] | **Paul Rulis**[1] | **Yuichi Ikuhara**[3,4] | **Isao Tanaka**[3,5]

[1]Department of Physics and Astronomy, University of Missouri-Kansas City, Kansas City, Missouri

[2]Department of Adaptive Machine Systems, Osaka University, Suita, Osaka, Japan

[3]Japan Fine Ceramics Center, Atsuta, Nagoya, Japan

[4]Institute of Engineering Innovation, University of Tokyo, Bunkyo, Tokyo, Japan

[5]Department of Materials Science and Engineering, Kyoto University, Kyoto, Japan

Correspondence
Wai-Yim Ching, Department of Physics and Astronomy, University of Missouri-Kansas City, Kansas City, MO, USA.
Email: chingw@umkc.edu

Funding information
DOE, Grant/Award Number: DE-FG0284DR45170, DE-AC03-76SF00098; the School of Graduate Studies at UMKC; Scientific Research on Innovative Areas "Nano Informatics", Grant/Award Number: 25106005; the Japan Society for the Promotion of Science (JSPS); Research Computing Support Services (RCSS) of the University of Missouri System

Abstract

Based on a previously constructed intergranular glassy film (IGF) model for bulk silicon nitride, a large periodic model of 3864 atoms containing 2 grains of different orientations from the main bulk β-Si_3N_4 and 2 IGFs was fully relaxed using the ab initio density-functional theory package VASP. The relaxed structure was then used to calculate the electronic structure, density of states, interatomic bonding, partial charge distribution, and electron localization using the OLCAO method. Analysis of the data focuses on the interfacial regions between bulk β-Si_3N_4 and the Si-O-N glass layer with different orientations. The total bond order density (TBOD) is evaluated in different interfacial and bulk regions. We show minor differences in the internal cohesion between crystalline grains of different facets. However, the overall charges in the bulk crystal grains and in the glassy regions are electropositive which are balanced by the negatively charged interfacial region between the two. The presence of a less rigid glassy layer is the reason for structural flexibility in ceramics without a huge penalty in the steric energy. The optimization of the interfacial structure and bonding via the creation of defective sites is the atomic origin for the existence of the IGF in silicon nitride. The insights obtained from this detailed quantum mechanical analysis of a realistic IGF model are discussed including implications on the strength, fracture toughness, and processing methods. We also discuss the potential applications of our method to other complex materials systems.

KEYWORDS

β-Si_3N_4, electronic structure, first-principle calculations, interatomic bonding, intergranular glassy film (IGF)

1 | INTRODUCTION

Silicon nitride (Si_3N_4), together with SiC and Al_2O_3 (and by extension to SiAlON), are generally considered to be the most important structural ceramics and have been at the core of ceramic research for over a century.[1-3] In recent years, there has been a concerted effort in the ceramic community to further extend and improve their processing, properties, and functionality so as to apply the ceramic materials at elevated temperatures or under harsh environment and at a reduced cost.[1-3] For effective industrial applications aiming at energy efficiency in many applications such as gas turbines, the brittleness and high-temperature degradation of the structural ceramics is an critical issue which can be overcome by effective control of microstructures and chemistry.[4-6] However, crystalline imperfections such as dislocations, grain boundaries (GBs), intergranular films (IGFs), and porosity cover an enormously vast and

complicated subject area that has been the center of research by both experimentalists and computational theorists.[1,4,6,7]

One of the defective structures that is ubiquitous in Si_3N_4 is a thin layer of glassy matter, approximately 1-3 nm thick, that is situated between different crystalline grains in the sintered samples.[7-10] These so-called intergranular glassy films (IGFs) are the key factor in controlling the mechanical properties of Si_3N_4. The glassy film contains a varying mixture of Si, O, and N with an almost constant thickness and the films intersect at triple junctions of the grains. A variety of experimental techniques have been used to investigate the structures of IGFs in Si_3N_4 including but not limited to HREM,[11] STEM[12] and ELNES.[13] These experimental efforts, in conjunction with computer simulations on IGF models to be described below, constituted the bulk of our current understanding of IGFs in Si_3N_4 but detailed information at the atomic scale is still very limited.

One of the most comprehensive modeling efforts using classical molecular dynamic (MD) simulations was accomplished by Yoshiya and coworkers beginning more than 15 years ago.[14-16] The effort resulted in a large periodic supercell IGF model that contains 2 bulk Si_3N_4 crystals that are rotated 90° with respect to each other. An IGF is inserted between each pair of facets of the crystalline grains. This model is a realistic representation of an IGF and it is consistent with experimental observations. A more detailed description of this model (hereafter referred to as the Yoshiya model) will be discussed in the next section. Some recent MD studies on IGFs in silicon nitrides with interests on fracture and impurity effects[17,18] should also be noted.

Computational modeling using classical MD has been very popular ever since its inception in the 1950s.[19-21] It had tremendous success in all areas of material research and it makes up a significant portion of all modeling efforts. MD can explore very large systems up to several million atoms and beyond.[22,23] It is also capable of exploring temperature dependencies and dynamic processes with long simulation sequences. A common feature in all MD simulation is the use of a classical, empirical potential function ranging from a simple Lennard-Jones type pair potential to a sophisticated, multiatom potential with numerous parameters that must be carefully calibrated. Thus, the efficiency and accuracy of MD simulations are to a large extent, dependent on the quality of the potential functions that are adopted. Significant effort must often be devoted to the development of potential functions relevant to the system under study. However, in recent times, it has become increasingly clear that development of such parameter-based potentials is either extremely difficult or effectively impossible for multicomponent systems or materials with highly complex structures. To this end, many groups have started to explore the use of ab initio methods usually based on the density functional theory (DFT) and in particular ab initio molecular dynamics (AIMD),[24] which can circumvent the difficulties faced by classical MD. The price to pay is that the system under study is usually limited to a few hundred atoms and with a severely limited time range because the computational cost is often 2-3 orders of magnitude greater than classical MD. However, the situation is partially ameliorated with the rapid advance of high performance computing (HPC) technology and the development of more efficient computational methods.

Ab initio studies of IGF models in Si_3N_4 have been performed by one of us (WYC) and his collaborators over the last 10 years.[25-29] The prior work focused on the interatomic bonding, mechanical properties evaluation, and fracture processes of the IGF under tensile strain. The model used in these earlier studies consisted of 907 atoms and the interfaces between the IGF and Si_3N_4 was restricted to the prismatic [0001] or basal plane of the hexagonal crystal of β-Si_3N_4, which is not fully realistic compared with the experimental reality. Nevertheless, those first-time ab initio IGF studies paved the way for understanding of the atomic-scale interactions based on quantum mechanical calculations and went beyond classical simulations where all the interpretations were based on geometric parameters.[10]

In this work, we used the Yoshiya model as the starting point and fully relaxed it using VASP (Vienna Ab initio Simulation Package).[30,31] We then used the orthogonalized linear combination of atomic orbital (OLCAO) method[32,33] to calculate the electronic structure and bonding. The results presented here include an analysis of the relaxed structure, the geometry at the interface, the interatomic bonding, the electronic structure, the localization of the state wave functions at the band edges, the partial charge distribution, and specific bonding features at the interface. These results enable us to reach some new conclusions and contribute to the development of a road map for connecting MD simulations with first principles calculations to bridge the length scale from the atomic or molecular scale to a larger meso-scale in materials simulations.

2 | EXTENSION OF THE YOSHIYA MODEL

The Yoshiya model[34] was originally generated by the simulated annealing method for MD simulation using the MOLDY code with the pair potential reported by Unuma[35] and with special precaution taken to maintain the integrity of the IGF model designed for the insertion of a Si-O-N glassy film between the 2 crystalline grains with a 90° twist. The resulting supercell model has 3864 atoms (1152

Si, 1536 N in the crystalline part and 432 Si, 240 N, and 504 O in the glassy region) with N/(N+O) ratio of 0.32[14,36] of which only a small fraction (<5%-10% of the glassy and interface regions) has dangling bonds at the interface.[34] There are 2 IGFs in the model oriented in the opposite direction in order to maintain the periodic boundary condition due to the twist of the crystalline grain. The size of the original model is 23.022Å × 23.028Å × 82.359 Å with the widths of the IGFs being about 13Å each.

The original Yoshiya model was then fully relaxed with high accuracy using VASP with no constraints to the volume or shape of the supercell using a large core configuration on NERSC supercomputer. We used the projector augmented wave (PAW) method and the PBE generalized gradient approximation (GGA) potential for exchange-correlation evaluation.[37,38] The electronic convergence limit was set at 10^{-5} eV and a high-energy cut-off of 500 eV was applied. A single k-point at Γ (0, 0, 0) was used for Brillion zone integration because the model is quite large. The VASP relaxation of the IGF model used a total of 96 hours with 82 nodes on the Cori machine at the National Energy Research Scientific Center (NERSC) at the Lawrence Berkeley Laboratory administered by the US Department of Energy.

The final supercell parameters of the relaxed Yoshiya model are a = 23.1412 Å, b = 23.1485 Å, c = 82.6135 Å, α = 90.008°, β = 89.805°, γ = 90.099°, which is close to the original Yoshiya model parallelepiped in shape with lattice constant expansion of <0.5% from the unrelaxed one. The ball and stick picture of the relaxed model is shown in Figure 1. Table 1 compares the cell parameters and the total energy of the unrelaxed Yoshiya model and the final, fully relaxed model. It is obvious that the relaxed model has slightly expanded supercell parameters compared with the unrelaxed model, despite that atoms are rearranged upon ab initio structure optimization. Those atoms form covalent and ionic bonds even between anions unlike in the classical MD case where the use of formal charge

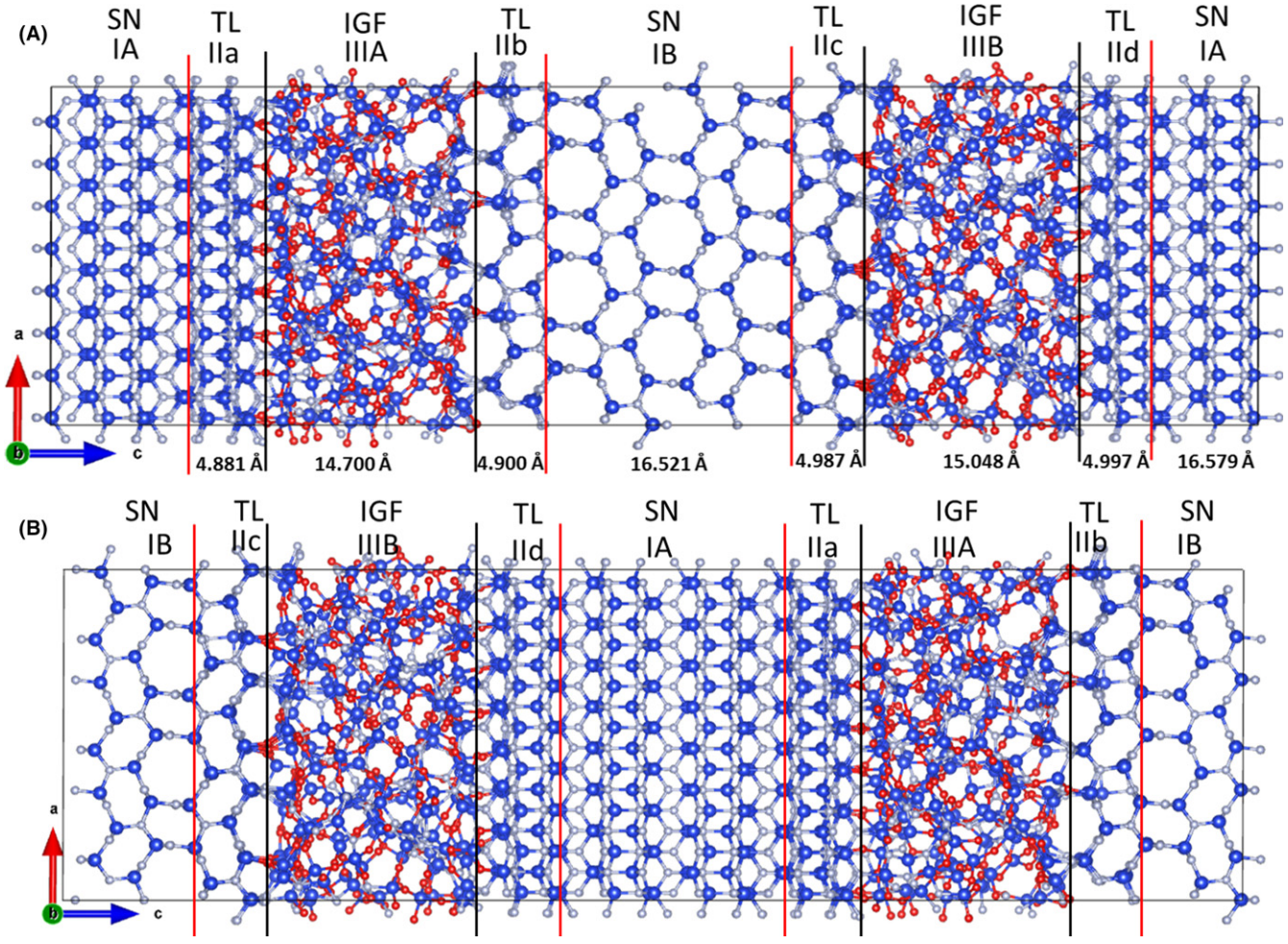

FIGURE 1 Ball and stick sketch of the relaxed Yoshiya model with the division into different regions and their width in Å. A, Centered at bulk crystal region IB and B, centered at bulk crystal region IA with a shift of 0.5 fractional coordinates from (A). Si: blue, N: gray and O: red

without charge transfer leads to a significant energy penalty.[32] It should be pointed out the total energy of the unrelaxed and relaxed models differ by 68.35 eV (or 0.0177 eV per atom) whereas the volume of the cell is increased by 591.86 (Å),[3] mostly from the movements of the atoms in the interfacial region.

In order to make a deeper analysis of the geometry and electronic structure of this relaxed IGF model is divided the model into 8 regions along the *c*-axis perpendicular to the IGF layer. They are labeled as bulk silicon nitride (SN) with 2 crystalline grains IA and IB, 2 IGF regions IIIA and IIIB, and 4 transition layers (TL) IIa, IIb, IIc, and IId corresponding the 4 transition layers between 2 bulk crystal and 2 IGF blocks. They are clearly illustrated in Figure 1A,B. In Table 2, we list the details of each region including the volume of the region, the number of each type of atoms and the ratio of N(N+O). The volume for each region is important in the later discussion of the internal cohesion of the grains using the total bond order density (TBOD) quantum mechanical metric. As will be clear in the next section, our careful division of the regions for the IGF model across the *c*-axis is highly conducive to the discussion of the fundamental interactions at the IGF interfaces, which has not been an easy task to discern.

The main effect of the accurate relaxation of the Yoshiya model was to define more precisely the different regions that were described above. Moreover, accurate identification of the over- and under-coordinated atoms in the IGF region and at the interfacial regions facilitate the understanding of the complex structure of IGFs in β-Si_3N_4. We should emphasize that the presence of these perceived defective sites are natural and they exist in real samples.[10,11] Precise identification and quantification of their locations are important for discussion of the roles that they may play in the electronic structure and bonding of the model, and their possible effect on the properties of IGFs as defective structures within the polycrystalline Si_3N_4 samples. Careful analysis of the relaxed structure shows that there are a considerable number of over- and undercoordinated Si and N ions, but only 2 undercoordinated O ions. This is shown in Figure 2 where we used the symbol "+" and "−" to denote that an atom is over- or undercoordinated. As can be seen, the defective atoms are located mostly in region IIa and IIIA and IIIA and IIb on the either side of the bulk IGF region (IIIA). Surprisingly, there is only one over-coordinated Si+ atom at the interface region IVa and all the N atoms are over-coordinated in both the interfaces and the interior of the glass region. Only 2 undercoordinated O atoms are identified in the bulk glassy region. So, almost all the defective sites possess dangling bonds, consistent with the description in Ref. (34) The same scenario occurs at the other interface/glassy region labeled as IIc-IIIB-IId on the other IGF IIIB in Figure 1.

3 | ELECTRONIC STRUCTURE AND INTERATOMIC BONDING

3.1 | OLCAO method, largest ab initio calculations

The electronic structure and interatomic bonding in the IGF model were calculated using the orthogonalized linear combination of atomic orbitals (OLCAO) method[33] using the atomic structure from VASP relaxation described above.

TABLE 1 Comparison of cell parameters and total energy of the unrelaxed and relaxed Yoshiya model

Supercell	a, b, c (Å)	α, β, γ	V (Å^3)	E(eV)
Unrelaxed	23.022, 23.028, 82.359	90.00°, 90.00°, 90.00°	43662.7	−31053.2
Relaxed	23.141, 23.149, 82.614	90.01°, 89.80°, 90.10°	44254.5	−31121.5

TABLE 2 Data for 8 regions. No of atoms (#atoms) for (Si, N, O), N/(N+O) ratio, Si/N ratio, Volume, No. of under and over coordinated atoms (#Un and #Ov)

Region	Width (Å)	#Total atoms	# N atoms	# O atoms	N/(N+O)	# Si atoms	V (Å^3)	#Un&Ov
IA	16.579	816	432	0	1.000	384	8881.1	0
IB	16.521	814	432	0	1.000	382	8850.2	0
IIa	4.881	265	166	3	0.982	96	2614.6	6
IIb	4.900	264	165	3	0.982	96	2624.9	3
IIc	4.987	265	166	1	0.994	98	2671.4	2
IId	4.997	267	168	3	0.982	96	2676.5	1
IIIA	14.700	587	125	246	0.337	216	7874.7	23
IIIB	15.048	586	122	248	0.328	216	8061.1	23
Total	82.614	3864	1776	504		1584	44254.5	58

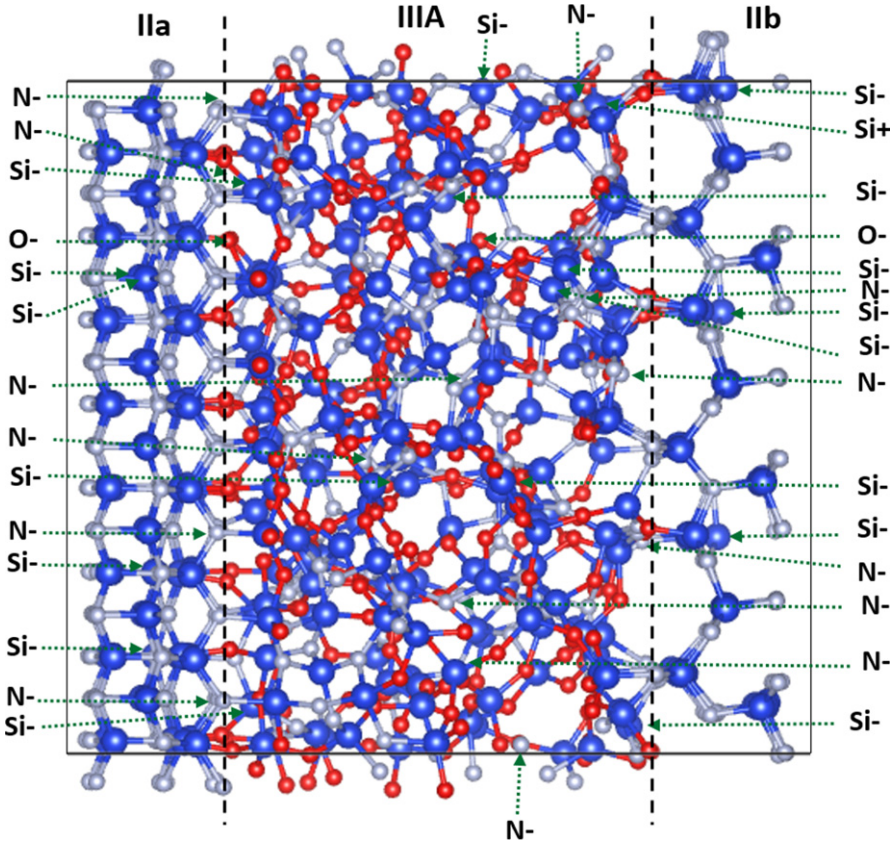

FIGURE 2 Enlarged figure for regions IIa, IIIA, IIb of Figure 1 showing the location of the over- and under coordinated atoms Si+, Si-, N+, N- and O+, O-

The OLCAO method uses atomic orbitals for the basis function expansion and is particularly effective for the electronic structure of large complex systems. The combination of VASP for structural optimization and OLCAO for properties evaluation has been successfully demonstrate in many crystalline[39-43] and noncrystalline materials,[44-48] and also in complex biomolecular systems.[49-53] In the present calculation, the basis consists of 1s, 2s, 2p, 3p, and 3d orbitals for Si and 1s, 2s, 2p orbitals for N and O. The dimension of the secular equation for this 3864 atom IGF model after orthogonalization against the core orbitals is 21316 × 21316. All of the energy eigenvalues and eigenvectors are available for detailed electronic structure and bonding analysis. For the OLCAO calculation and analysis of the results, we used a single core with large memory on the Lewis cluster at the University of Missouri for various parts of the calculation and analysis which took <10 calendar days to complete.

Central to the analysis of the electronic structure is the calculation of the effective charge Q^*_α and the bond order $\rho_{\alpha\beta}$ between all pairs of atoms (α, β) within the model. They are calculated based on the Mulliken scheme[54,55] using a minimal basis according to the following two formulas.

$$Q^*_\alpha = \sum_i \sum_{m,occ} \sum_{j,\beta} C^{*m}_{i\alpha}\, C^{m}_{j\beta}\, S_{i\alpha,j\beta} \qquad (1)$$

$$\rho_{\alpha\beta} = \sum_{m.occ} \sum_{i,j,} C^{*m}_{i\alpha} C^{m}_{j\beta} S_{i\alpha,j\beta} \qquad (2)$$

Here, $S_{i\alpha,\ j\beta}$ are the overlap integrals and the C's are coefficients of the system eigenvectors. All quantities are real numbers because the diagonalization of the secular equation was carried out only at the k = (0,0,0) point.

The TBOD is an important quantum mechanical metric to assess the internal cohesion and strength of a material. It is obtained by summing up all bond order pairs in the model and then normalized by the volume of the model. In the present study, the key issue is to obtain the TBOD for each region defined in Figure 1 since both the BO values and the volumes are exactly defined in those regions. This is the most innovative way to analyze the effect of the IGF and its interaction with the crystalline grain. This will be discussed in more detail in section 3.5.

3.2 | Density of states and partial density of states

The calculated total density of states (TDOS) for the relaxed Yoshiya model is shown in Figure 3. The calculated band gap for the model is 1.6 eV, much less than the band gap of 4.96 eV for β-Si_3N_4[56] and 5.20 eV for amorphous SiO_2 using the same method.[44] The general features of the TDOS are unremarkable. The valence band (VB) consists of a lower portion and an upper portion separated

by a gap of about 1.6 eV, similar to those in β- Si_3N_4 and a-SiO_2. In the present case of the IGF model, the TDOS consists of a mixture of contributions from bulk Si_3N_4 portion, the inter-granular glassy region, and the interfacial layers between the two. To look into more details at the difference in the DOS from different regions, we display the partial DOS (PDOS) for each region of IA, IB, II, and III in Figure 4A,B with different energy ranges. Region IA and IB are the 2 bulk regions with different orientations at the interface. Region III (IIIA + IIIB) are the interior of the glassy region; and region II (IIa + IIb + IIc + IId) represent the transition layers between glass and the bulk crystal with different facet. It is quite striking to see that there are virtually no differences in the PDOS from the 4 regions. The only clear difference is in the lower part of the VB where regions II and III differ from regions IA and IB. This difference originates from the presence of O atoms in the former because O-2s levels are lower than N-2s levels. There is virtually no difference in the conduction band (CB) region both in the shape and peak structures. This is probably because all states in the CB are delocalized and are not sensitive to any structural differences in the different regions of the IGF model. (See next section).

In Figure 5, we separately display the PDOS of the glassy region III with decomposition into atomic components of Si, N, and O. There is virtually no difference for PDOS from regions IIIA and IIIB, or due to the difference in the orientations with the crystalline facets. Simply said,

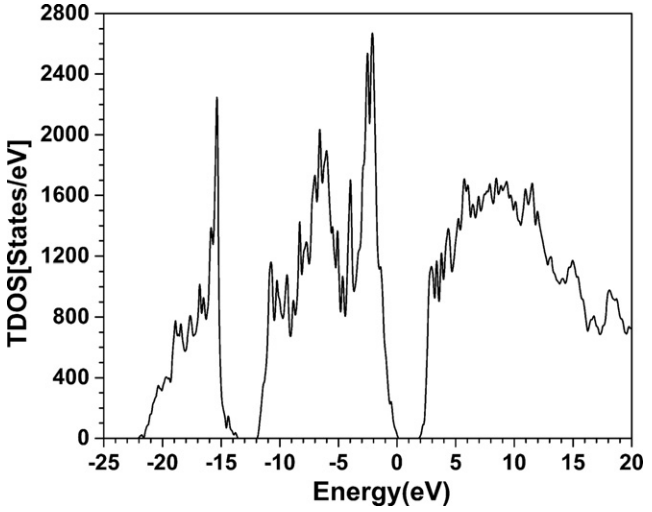

FIGURE 3 TDOS of the relaxed Yoshiya model

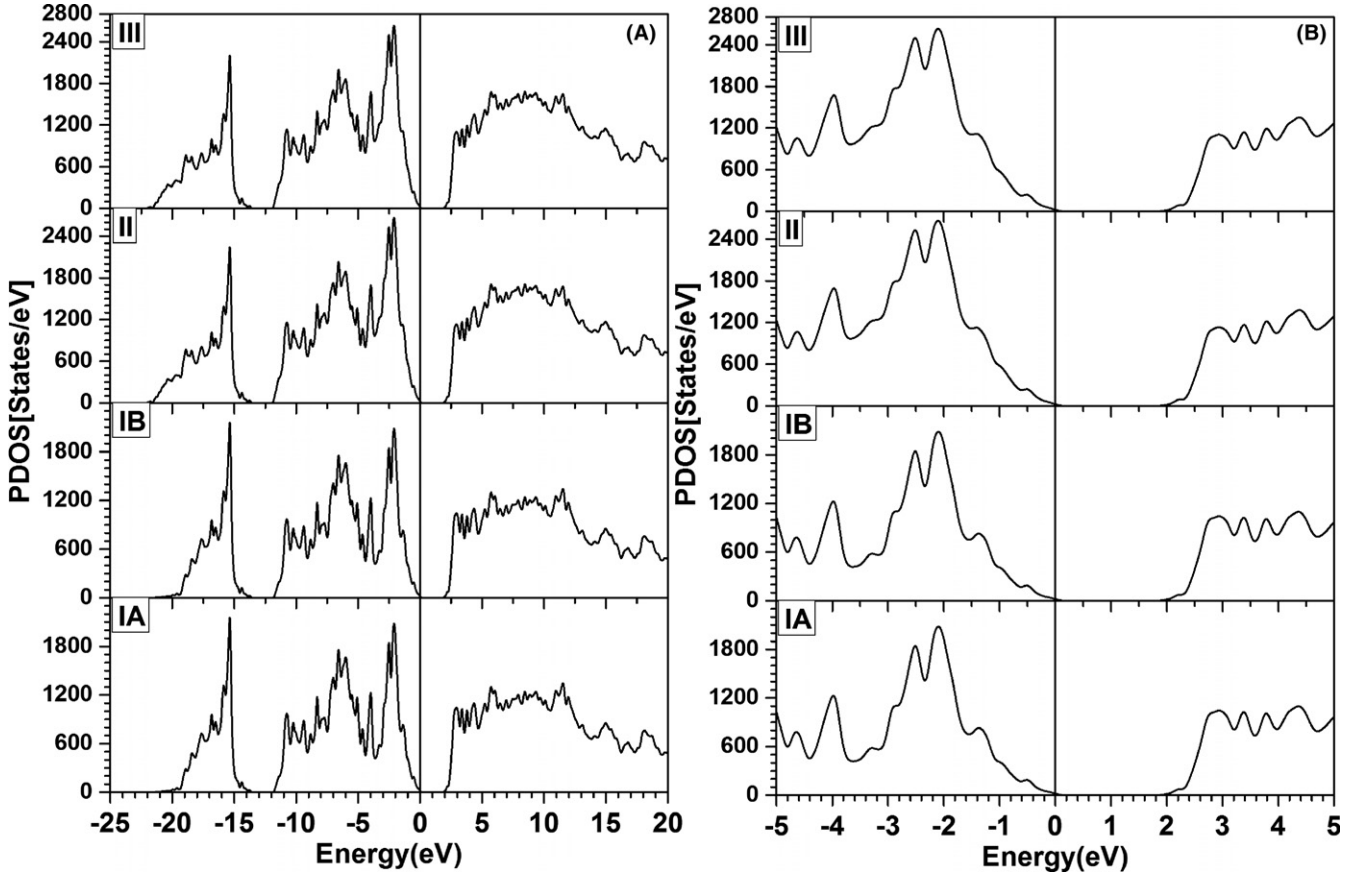

FIGURE 4 Calculated PDOS of the relaxed Yoshiya model for the 4 regions IA, IB, II, and III. A, From −25 to 20 eV; B, from −5 eV to 5 eV

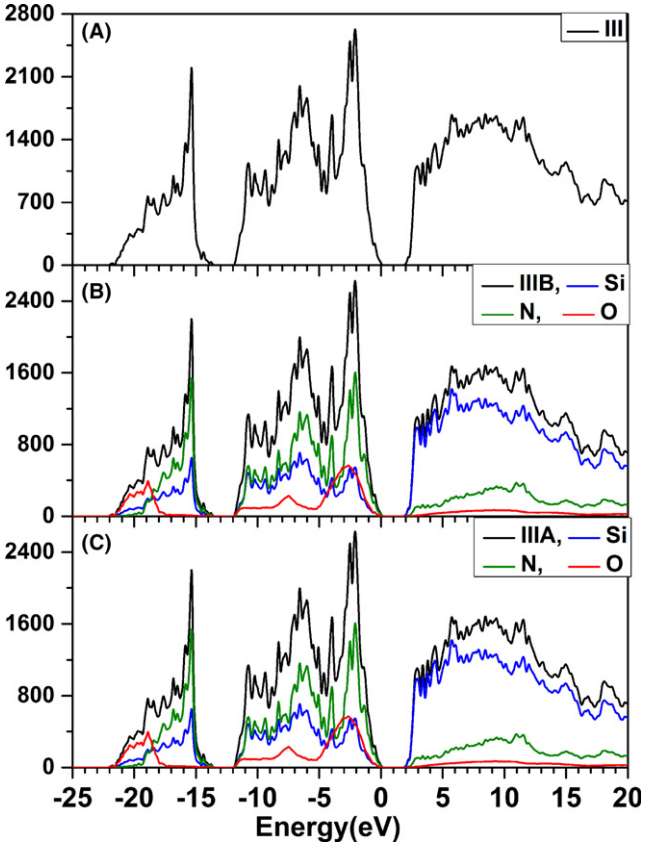

FIGURE 5 PDOS of the IGF part (region III, IIIA and IIIB) of the relaxed Yoshiya model. The atom-resolved PDOS is shown in color: Si: Blue, N: green, O: red

the DOS or PDOS is a more averaged electronic property not sufficiently sensitive to the small variations in the structure of a complex material such as IGF in structural ceramics. In other words, even when structure is defective, atoms are rearranged to form similar valence band to those in nondefective structure.

3.3 | Localization index

In a noncrystalline disordered system described by a large structure model of N atoms, it is quite common to calculate the localization index $(LI)_m$ for each state m of the model according to:

$$LI_m = \sum_{i,\alpha}\left[\sum_{j,\beta} C^{*m}_{i,\alpha} C^{m}_{j,\beta} S_{i\alpha,j\beta}\right]^2 \quad (3)$$

$(LI)_m$ designates the degree of localization for the wave functions of the states shown in the DOS and can be quite useful in the discussion on the electron transport properties. LI ranges from 1 to 1/N for a completely localized state on 1 orbital of 1 atom to a completely delocalized stated spread evenly on all N orbitals of all atoms. Obviously the larger the model the more realistic the calculated LI.

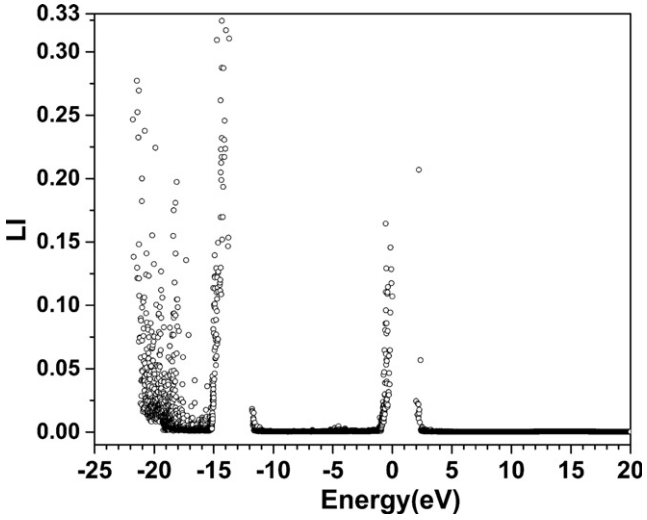

FIGURE 6 Localization index (LI) of the relaxed Yoshiya model

Figure 6 shows the calculated localization index for the relaxed Yoshiya model. As expected the states at the band edges, both the upper and lower VB are highly localized whereas the states in the CB or in the middle of the upper VB are completely delocalized which resulted in the no difference in CB DOS discussed above. There are a few states at the bottom of the CB that are highly localized; some of them originate from the "defective" atoms with dangling bonds. It is also noted that the states in the lower VB are all significantly localized especially at the lower parts of the VB. These states originate from the O atoms in the IGF region (see Figure 5).

3.4 | Effective charge distributions

The effective charges Q^*_α on every atom α in the IGF model are calculated according to Equation (1) and displayed against the position on the *c*-axis in Figure 7. What is plotted in Figure 7 is actually the partial charge ΔQ^*, or the deviation of the effective charge Q^* from the neutral atom with charge Q^0.

Thus, $\Delta Q^* = Q^0 - Q^*$. ΔQ^* is positive in Si which means it loses charge. $\Delta Q^*$are negative for O and N which gain electrons from Si. It can be seen that there are large deviations in ΔQ^* in the IGF and in transition layers but it remains more or less constant in the bulk crystalline region as expected. However, on a closer inspection, the variations in the bulk region are somewhat graded over several layers of crystal planes away from the interface boundaries. Purely classical simulations cannot reveal such details. The average ΔQ^* values for Si, N, and O are 1.28, −0.93, and −0.76 electrons respectively. N atoms are more electronegative than O when it comes to gaining electrons from Si. It can also be seen that the fluctuations in $\Delta Q^*$are larger for the N atoms in the glassy and interface regions. Of

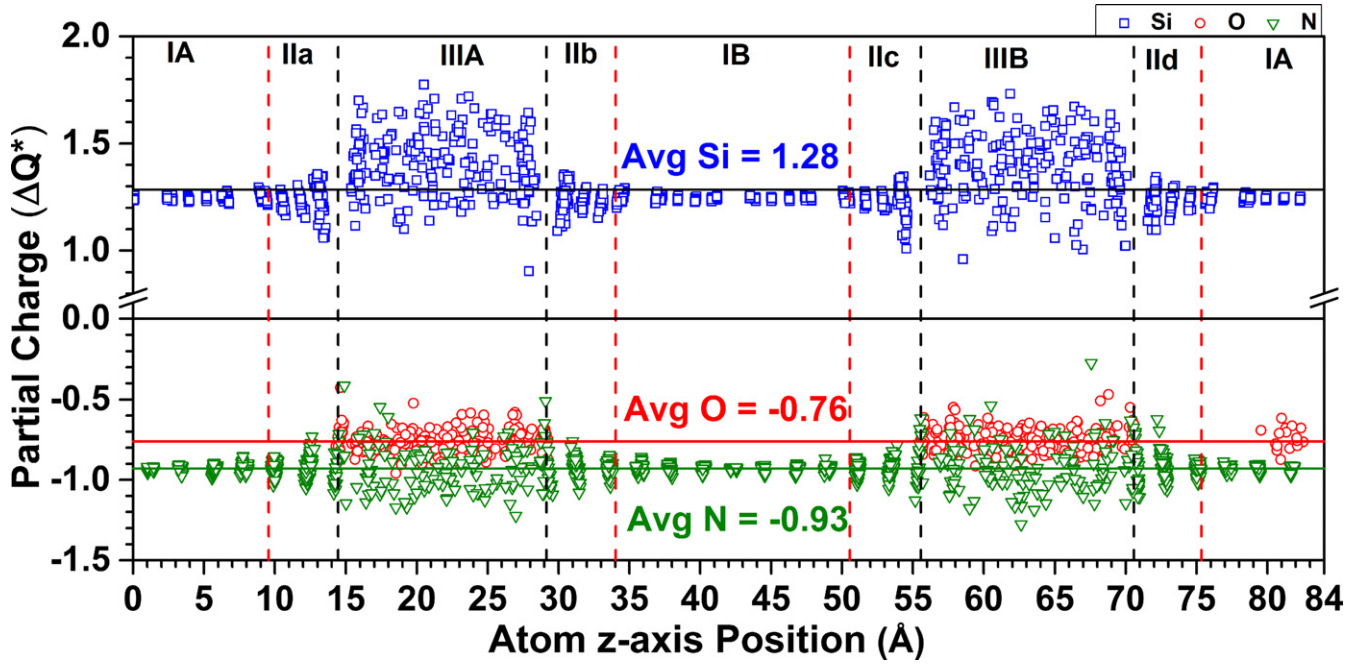

FIGURE 7 Partial Charge (ΔQ*) distribution for all the atoms in the relaxed Yoshiya model across the z-axis in different regions according to Figure 1(A)

TABLE 3 Summary of bonding and partial charge distribution in the IGF model

Region	IA	IB	IIa	IIb	IIc	IId	IIIA	IIIB	Entire-IGF
Vol (Å^3)	8881.1	8850.2	2614.6	2624.9	2671.4	2676.5	7874.7	8061.1	44254.5
ΔQ*	75.350	72.808	−38.578	−37.043	−33.978	−39.984	0.099	1.326	0.001
PBO									
Si-O	-	-	4.0496	3.38845	4.08855	3.4543	152.9138	153.2031	0.0073
Si-N	525.7126	524.2523	157.9385	158.5688	158.9886	160.152	129.8809	128.6283	0.0439
O-O	-	-	-	-	-	-	0.004	-	0.0000
N-O	-	-	-	-	-	-	0.0034	-	0.0000
TBO	525.7126	524.2523	161.9881	161.9572	163.0771	163.6063	282.8020	281.8314	2265.2254
TBOD	0.0592	0.0592	0.0620	0.0617	0.0610	0.0611	0.0359	0.0350	0.0512

course, these N atoms are the undercoordinated atoms at the interface of the transition layers or in the glassy regions as shown in Figure 2. It is also clear that the average ΔQ* for Si is much larger in the interface and glass region than in the bulk crystalline grains.

The total partial charge ΔQ* for each region in the IGF model is listed in Table 3. It is apparent that the partial BO for Si-O bonds are much smaller in the transition layers (IIa, IIb, IIc, and IId) than in the interior of the IGF region (IIIA and IIIB), since the later contains most of the Si-O bonds in the entire IGF model.

Table 3 also shows that the bulk crystal grain with prismatic facets (region IA) has total partial charge of 75.35 electrons, larger than the other twisted grain (region IB 72.81 electrons) by 2.54 electrons, and that the 2 glassy regions with opposite orientations (region IIIA and IIIB) also have positive partial charges of 0.099 and 1.326 electrons respectively. The balance of the partial charge comes from the interfacial regions (IIa + IIb) and (IIc + IId) which have negative partial charges of −75.62 and −73.96 electrons respectively. Combining these data together, we obtain some very important insights. In polycrystalline ceramics, both the bulk grains and the IGF are positively charged but their interfaces tend to be negatively charged due to charge transfer. This results in an electrostatic attraction between the glass region and the bulk crystalline grain, which tends to facilitate the formation of the IGF. As crystalline grains covered by glassy oxides gradually come close to each other during sintering, the glass-crystal interfaces will increasingly repel each other electrostatically.

Eventually, equilibrium is reached whereby the interfacial repulsion is balanced by the interface-glass and interface-bulk attractions. Moreover, this is the first solid evidence that the orientation of crystalline faces do make some difference. One of the 2 twisted crystal grains has less charge transfer than the other one.

3.5 | Interatomic bonding quantified by bond order

The bond order (BO) values between every pairs of atoms in the IGF model are calculated according to Equation (2) using the OLCAO method. They are displayed in the form of a scatter-plot of BO vs bond length (BL) up to 2.0 Å in Figure 8. Because highly covalent Si-N bonds are stronger than the Si-O bonds, which have a large ionic component, the BO values for Si-N bond are larger than the Si-O bond. These BO values generally scale with BL but more so in Si-N bonds than in Si-O bonds. Figure 8A shows a large concentration of the Si-N BO values clustered around 1.74 Å to 1.76 Å. These are from bond pairs in the crystalline region. Similarly, there is a relative large cluster of Si-O bonds around 1.62 Å to 1.64 Å. They come from the Si-O bonds in the interior part of the glass region where the distortion in Si-O bond lengths are less than for O atoms close to the interface region. To unmask the BO distribution for bond pairs in the interfacial region, we subtracted the BO data in the regions I, which correspond to the BO values from the bulk crystalline region. The results are shown in Figure 8B. Data for Si-O and Si-N pairs in region II (transition layer) and region III (IGF) are distinguished by different color and symbols. Several marked observations are clear. (i) They are widely scattered. (ii) They consist of data points of high and low BO values, or equivalently, they contain most of the strongly bonded and weakly bonded pairs in the IGF model caused by geometric distortions for atoms at the interface. (iii) The variations in the BO vs BL are more pronounced in Si-N bonds (squares) than in Si-O bonds (circles). We can roughly divide them in 2 types, high BO and weaker BO for both Si-N, and Si-O bonds as, light-blue for Si-N bonds and pink for Si-O bonds. For Si-N bonds, the strong bonds scale with their BL but this is not so with the weaker bonds. For the Si-O bonds, they scale with BL very slowly and with less data for BL greater than 1.8 Å. All these plots show that ab initio calculations can reveal intimate details of interatomic bonding in the IGF model in Si_3N_4.

3.6 | TBOD and PBOD

The plots of BO vs BL in the IGF model reveal the distribution of the scattered data in the model. However, what is less clear is what they can reveal about the bond strength or cohesion in different regions of the IGF along the c-axis. To investigate this important question, we make use of the concept of the TBOD alluded to earlier in section 3.1. First, we plot the same data in Figure 8A along the *c*-axis as shown in Figure 9A.

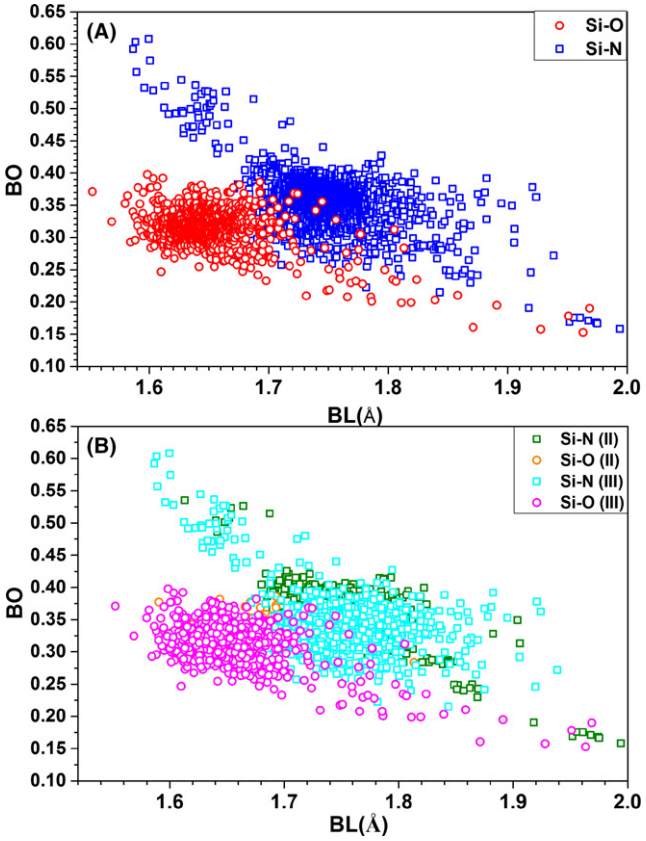

FIGURE 8 A, BO vs BL distributions for all atomic pairs in the relaxed Yoshiya model. B, The same plot as in (a) except those bond pairs from the bulk region are removed showing on those in the IGF (region III) an in the transition layer (region II)

It reaffirms the observation made in the previous section that the stronger and weaker bonds all occur at the interfacial region and in the glassy region. The bond strengths are uniform within the bulk crystalline region. Next, we divide the cell into slices along the *c*-axis that are 2.5 Å thick. Because we have the precise volume and the BOs within each region, we can calculate the TBOD within each slice. The results for the TBO, average BO, standard deviation of the BO and PBOD within each slice are shown in the 4 horizontal panels below the BO distribution. Figure 9B shows the same plot as in Figure 9A except they are positioned with different centers (IIIA and IIIB) at the middle of the plot along the *c*-axis. The last row in Figure 9 are similar to that of Figure 1 for easy comparison. It clearly shows that the bulk region has the highest average TBOD, which is expected because they are populated with perfect, strong

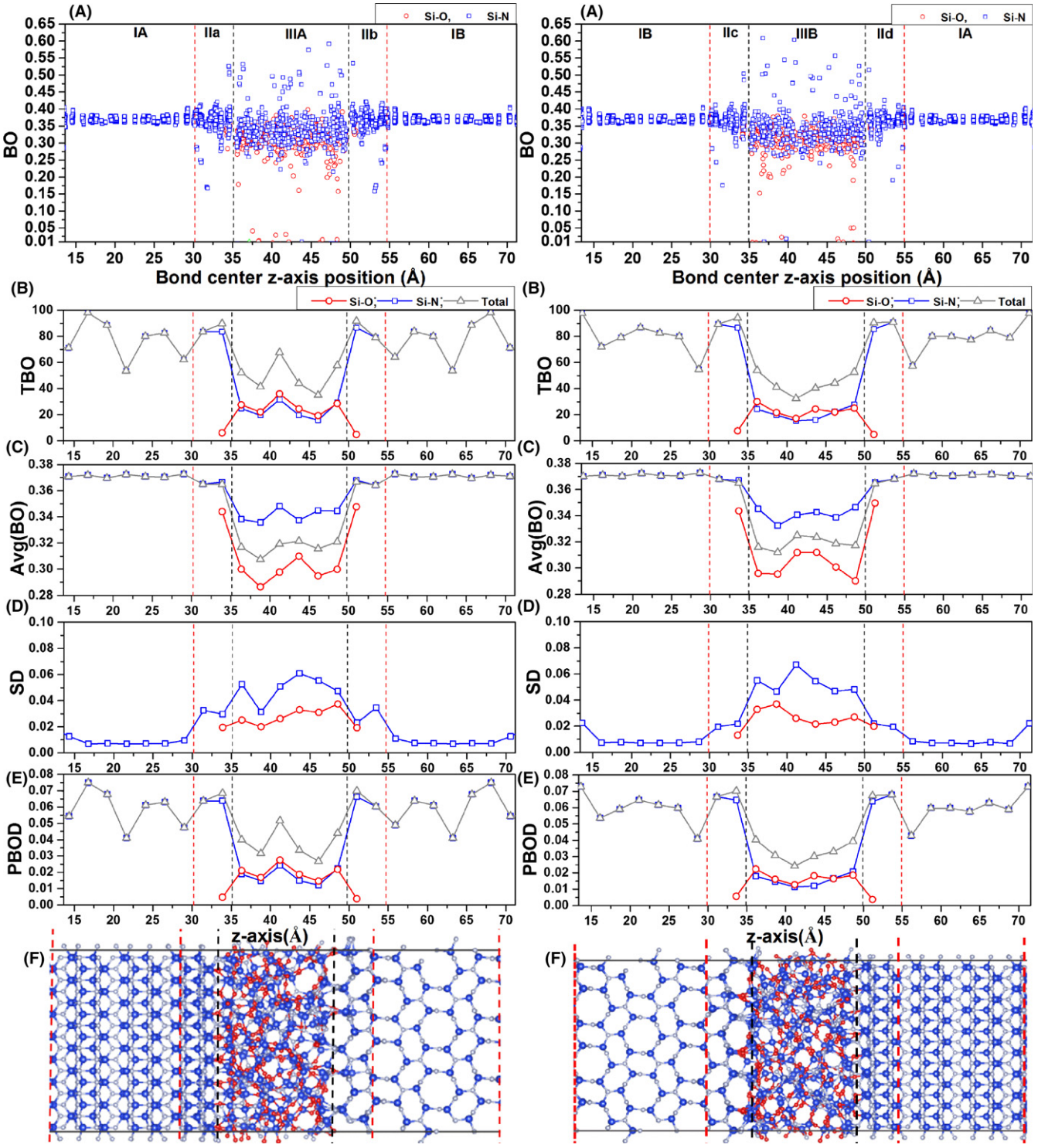

FIGURE 9 Left column: A, Bond order distribution across different regions of the IGF model, B, total bond order (TBO), C, average bond order (Avg(BO)), D, standard deviation (SD) of bond order, E, partial bond order density (PBOD), and F, ball and stick figure, along z-axis. Right column: Same as left column with a shift of 0.5 fractional coordinate such that the 2 differently oriented region are on the opposite side

Si-N bonds. What is surprising is that the TBOD at the interface region is comparable to that in the glassy region. This new finding gives the necessary insights about the relative strength of the interior of the glass region vs the interface regions that adjoin the crystalline facets of different orientation. Furthermore, this provides hints about the fundamental reason for the formation of IGFs as will be discussed in the next section.

4 | DISCUSSION

The results described above for a very large ab initio DFT calculation on a realistic IGF model imply first that such calculations are clearly now possible and that they will hopefully become more common in the future. The results of ab initio calculations on systems that accurately model realistic defective structures obtained from traditional MD simulations of up to several thousand atoms may provide a crucial link between atomic/molecular scale calculations to meso-scale calculations. Such a link will be important in the development of predictive multiscale modeling which can account the longer range structures than purely based on ab initio simulations. Over the last 2 decades, various techniques and schemes have been developed and implemented but few have really succeeded in the way they intended. These include the divide and conquer technique,[57] or an approach of focusing in a small fragment of a large model for ab initio treatment that is key to the solution and find ingenious ways to make smooth connections at their boundaries etc. The ability to do ab initio calculations for the entire large model can certainly mitigate many of the drawbacks that arise from the associated approximations introduced in those schemes.

In the present application to the Yoshia IGF model, several interesting and previously unknown facts have been revealed. Firstly, we explored the effect of different facet orientations of the crystalline grain within a single model, prismatic vs 90° twist on the electronic structure of the IGF. They show some subtle differences especially in the partial charge results. These minor differences indicate that the structural modification of facet orientation can be accommodated by an adjustment of the interfacial structure by accurate relaxation using ab initio methods, a feat that cannot be accomplished by classical MD because the potential functions used in classical MD are fixed and cannot reflect the minor electronic structure differences. Second, the exact role played by the presence of defective atoms with imperfect local bonding in the IGF was revealed in quantitative detail in the form of partial charge and bond order calculations. To what extent these nonideal bonding patterns affect the strength of the IGF in structural ceramics has been the source of much debate.

Most importantly, this work demonstrated the effective use of the new concept of TBOD in assessing the strength and weakness of the structure of different components of the structure. By dividing the IGF model in into different segments, bulk, glassy, transition layer and interface, we obtain the reliable quantities on TBOD. This is because both the TBO and the volume for each segment are exactly defined without any ambiguity. This is very different from traditional descriptions of interfacial effect in term of only geometric parameters such as bond lengths or bond angles of the atoms involved. It should also be pointed out that even in many ab initio simulations, the structural stability is usually assessed by comparing the total energies or formation energy. Obviously, it is not possible to apply such scheme to different regions of the IGF model nor is it computationally feasible for a large model such as the one used here. Another important advantage of using the TBOD concept is that it can be applied to different IGF or grain-boundary (GB) models with different structures and compositions. This is because the concept of TBOD does not specifically depend on the details of the materials under study, as long as the interatomic BO values are calculated using the same basis set within a single method.

Related to BO and TBOD, the calculation of the total partial charge or ΔQ^* in different parts of the Yoshiya model provided the first insight of the origin of the formation of the IGF in polycrystalline ceramics based purely on the atomistic quantum calculations which is difficult to obtain by classical methods. The total partial charges for different parts of the IGF model enable us to gain insights based on the electrostatic attraction or repulsion between different structural components in such structures based on first principles calculations.

The results provided above have implication on fracture of the sample due to interfacial bonding or debonding and the overall mechanical properties of structural ceramics. Based on the quantitative evaluations of the TBOD in the model, it is easy to conclude that the fracture of the structural ceramics is rooted in the presence of the glass film itself because the bulk glass region has the lowest TBOD. The interfacial regions with the bulk crystal play a relatively minor role. This is because Si-O bonds in the glass region are weaker than Si-N bonds in the bulk grains. They are not much affected by the defective structures, which are always present in both the glassy structure and at the interfacial region. This is consistent with one of our earlier studies on the smaller prismatic model of IGF where a tensile simulation experiment clearly shows the breaking is at the interior of the glassy region, not initiated at the interface.[28]

Of course this is valid only for an idealized case in which the sample is composed only of Si, N, and O in which the solubility of Si_3N_4 in the glassy layer is determined by thermal equilibrium at the sintering temperature[58] as in the case of samples sintered without additives.[59] Absence of any shear component of stress and residual stress are also an overly simplified assumption to discuss the fracture of polycrystalline materials. There have been many experimental endeavors[9-13] devoted to understand the effects of dopants on the fracture strength of IGF, since some dopants are segregated within the IGF or the IGF-crystal interface. They typically reduce the interfacial fracture strength and thereby increasing the fracture toughness by grain-bridging mechanism.

S. Ii et al[60,61] has studied the crack propagation at the interface of Si_3N_4 grain and IGF using high-resolution TEM and observed that the crack path was atomically flat at the boundary. This appears to be not in line with the BO analysis in the present work. There could be many possible reasons. BO measures static strength of bonds. Response of BO to the external complex stress should be taken into account in order to discuss the crack propagation path. Macroscopic residual stress that could occur near the IGF when the samples are sintered at high temperatures and cooled down to room temperature may strongly affect the crack path. The 90° twisted prismatic IGF model is just one example of possible IGFs. Statistical analyses for many different boundaries should be taken into account. Furthermore, in real ceramic material, presence of unknown impurities and/or atomic defects may be localized in IGF or TL, which may also affect the crack propagation path.

5 | CONCLUSION

In summary, we have presented detailed results of electronic structure and interatomic bonding in a large and realistic model of an intergranular glassy film in Si_3N_4. Our results reveal many new insights about the IGF structure and its properties. The most important one is the quantitative evaluations of the strength and cohesion of different regions of the IGF via the accurate calculation of the TBOD for each region. We have also shown from the partial charge calculation that the crystalline facet orientation does make some difference on the local charged grains. The fact that both the crystalline grain and bulk glass region have positive charges balanced by large negative charges at their boundary that affect the long-range electrostatic interaction in the sintering process. The insight obtained on the interatomic bonding and partial charge distribution in IGF offers plausible explanation on the atomistic origin of their properties and suggest possible means of enhancement such as specific addition of other elements at the interface for the structural ceramics.

Based on the opportunities presented by the present work, further research on complex ceramic materials and their composites can be contemplated using large scale ab initio calculation as a tool that is capable of approaching the mesoscale limit in multiscale modeling. Examples of such endeavors include the doping of different rare earth elements in IGFs and their segregation behavior to the interface similar to those of grain boundaries in alumina.[62,63] Further simulations on such large models based on compression and tensile extension can provide new information about the fracture mechanics and useful parameters for continuum level modeling. The method and approach we suggested and successfully implemented can be applied to systems that are not restricted to traditional structural ceramics. For example, it can be used to explore the role of alkali doing or mixed doping in silicate glasses,[48] strengthening of Ni-based super alloys, Inconel740 and Haynes282 by strategic inclusion of precipitate phases, or even organic or biological elements such as peptides in conjunction with crystalline calcium carbonate crystals as part of nature inspired materials,[64] insertion of crystallites of metallic alloys in bulk metallic glasses[65] etc. The opportunities are unlimited.

ACKNOWLEDGMENTS

WC and PR were supported by DOE DE-FG0284DR45170 in the past when this work was initiated. PA is supported in part by a grant from the School of Graduate Studies at UMKC. MY and IT were supported by a Grant in Aid for Scientific Research on Innovative Areas “Nano Informatics” (Grant No. 25106005) from the Japan Society for the Promotion of Science (JSPS). PA is supported by a research grant from the School of Graduate Studies at UMKC. This research used the resources of the National Energy Research Scientific Computing Center supported by DOE under Contract No. DE-AC03-76SF00098 and the by Research Computing Support Services (RCSS) of the University of Missouri System.

ORCID

Wai-Yim Ching http://orcid.org/0000-0001-7738-8822

REFERENCES

1. Hampshire S. Silicon nitride ceramics. In: Ohji T, Singh M, eds. *Engineered Ceramics*. Hoboken, NJ: John Wiley & Sons, Inc.; 2016:77-97.
2. Klemm H. Silicon nitride for high-temperature applications. *J Am Ceram Soc*. 2010;93:1501-1522.
3. Hoffmann MJ, Fünfschilling S, Kahraman D. Hot isostatic pressing and gas-pressure sintering. In: Riedel R, Chen I-W, eds. *Ceramics Science and Technology*. Weinheim, Germany: Wiley-VCH Verlag GmbH & Co. KGaA; 2012:171-187.
4. Becher PF, Sun EY, Plucknett KP, et al. Microstructural design of silicon nitride with improved fracture toughness: I, effects of grain shape and size. *J Am Ceram Soc*. 1998;81:2821-2830.
5. Hoffmann MJ. Analysis of microstructural development and mechanical properties of si3n4 ceramics. In: Hoffmann MJ, Petzow G, eds. *Tailoring of Mechanical Properties of Si3n4 ceramics*. Dordrecht, Netherlands: Springer; 1994:59-72.
6. Tanaka I, Pezzotti G, Matsushita KI, Miyamoto Y, Okamoto T. Impurity-enhanced intergranular cavity formation in silicon nitride at high temperatures. *J Am Ceram Soc*. 1991;74:752-759.
7. Clarke DR. On the equilibrium thickness of intergranular glass phases in ceramic materials. *J Am Ceram Soc*. 1987;70:15-22.

8. Kleebe H-J, Hoffmann M, Rühle M. Infuence of secondary phase chemistry on grain boundary film thickness in silicon nitride. *Z Metallked*. 1992;83:610-617.
9. Tanaka I, Kleebe HJ, Cinibulk MK, Bruley J, Clarke DR, Ruhle M. Calcium concentration dependence of the intergranular film thickness in silicon nitride. *J Am Ceram Soc*. 1994;77:911-914.
10. Subramaniam A, Koch CT, Cannon RM, Rühle M. Intergranular glassy films: an overview. *Mater Sci Eng, A*. 2006;422:3-18.
11. Kleebe H-J. Structure and chemistry of interfaces in si3n4 ceramics studied by transmission electron microscopy. *J Ceram Soc Japan*. 1997;105:453-475.
12. Shibata N, Pennycook SJ, Gosnell TR, Painter GS, Shelton WA, Becher PF. Observation of rare-earth segregation in silicon nitride ceramics at subnanometre dimensions. *Nature*. 2004;428:730-733.
13. Gu H, Tanaka I, Cannon RM, Pan X, Rühle M. Inter-granular glassy phases in the low-cao-doped hiped si3n4 ceramics: a review. *Int J Mater Res*. 2010;101:66-74.
14. Yoshiya M, Adachi H, Tanaka I. Interpretation of si-l2, 3 edge electron energy loss near edge structures (elnes) from intergranular glassy film of si3n4 ceramics. *J Am Ceram Soc*. 1999;82:3231-3236.
15. Yoshiya M, Tanaka I, Adachi H. Energetical role of modeled intergranular glassy film in si 3 n 4–sio 2 ceramics. *Acta Mater*. 2000;48:4641-4645.
16. Yoshiya M, Tatsumi K, Tanaka I, Adachi H. Theoretical study on the chemistry of intergranular glassy film in si3n4–sio2 ceramics. *J Am Ceram Soc*. 2002;85:109-112.
17. Zhang S, Garofalini SH. Effect of thickness of the intergranular film on fracture in si3n4. *J Am Ceram Soc*. 2009;92:147-151.
18. Jiang Y, Garofalini SH. Role of lu and la in the intergranular films on growth of the prism surface in β-si 3 n 4: a molecular dynamics study. *Scr Mater*. 2016;113:97-100.
19. Metropolis N, Rosenbluth AW, Rosenbluth MN, Teller AH, Teller E. Equation of state calculations by fast computing machines. *J Chem Phys*. 1953;21:1087-1092.
20. Alder BJ, Wainwright TE. Studies in molecular dynamics. I. General method. *J Chem Phys*. 1959;31:459-466.
21. Rahman A. Correlations in the motion of atoms in liquid argon. *Phys Rev*. 1964;136(2A):A405-A411.
22. Shibuta Y, Oguchi K, Takaki T, Ohno M. Homogeneous nucleation and microstructure evolution in million-atom molecular dynamics simulation. *Sci Rep*. 2015;5:1-9.
23. Germann TC, Kadau K. Trillion-atom molecular dynamics becomes a reality. *Int J Mod Phys C*. 2008;19:1315-1319.
24. Marx D, Hutter J. *Ab Initio Molecular Dynamics: Basic Theory and Advanced Methods*. Cambridge, UK: Cambridge University Press; 2009.
25. Rulis P, Chen J, Ouyang L, Ching W-Y, Su X, Garofalini S. Electronic structure and bonding of intergranular glassy films in polycrystalline si 3 n 4: Ab initio studies and classical molecular dynamics simulations. *Phys Rev B*. 2005;71:235317.
26. Ching W, Chen J, Rulis P, Ouyang L, Misra A. Ab initio modeling of clean and y-doped grain boundaries in alumina and intergranular glassy films (igf) in β-si3n4. *J Mater Sci*. 2006;41:5061-5067.
27. Misra A, Ouyang L, Chen J, Ching W. Ab initio calculations of strain fields and failure patterns in silicon nitride intergranular glassy films. *Philos Mag*. 2007;87:3839-3852.
28. Ching W, Rulis P, Ouyang L, Misra A. Ab initio tensile experiment on a model of an intergranular glassy film in β-si 3 n 4 with prismatic surfaces. *Appl Phys Lett*. 2009;94:051907.
29. Ching W, Rulis P, Ouyang L, Aryal S, Misra A. Theoretical study of the elasticity, mechanical behavior, electronic structure, interatomic bonding, and dielectric function of an intergranular glassy film model in prismatic β-si 3 n 4. *Phys Rev B*. 2010;81:214120.
30. Kresse G, Furthmüller J. *Vienna ab-initio simulation package (vasp)*. Vienna, Austria: Vienna University; 2001.
31. Kresse G, Furthmüller J. Efficient iterative schemes for ab initio total-energy calculations using a plane-wave basis set. *Phys Rev B*. 1996;54:11169.
32. Ching W. Theoretical studies of the electronic properties of ceramic materials. *J Am Ceram Soc*. 1990;73:3135-3160.
33. Ching W-Y, Rulis P. *Electronic structure methods for complex materials: The orthogonalized linear combination of atomic orbitals*. Oxford, UK: Oxford University Press; 2012.
34. Yoshiya M, Tanaka I, Adachi H, Cannon RM. Theoretical study on the structure and energetics of intergranular glassy film in si3n4-sio2 ceramics. *Int J Mater Res*. 2010;101:57-65.
35. Unuma H, Kawamura K, Sawaguchi N, Maekawa H, Yokokawa T. Molecular dynamics study of na-si-o-n oxynitride glasses. *J Am Ceram Soc*. 1993;76:1308-1312.
36. Gu H, Cannon R, Rühle M. Composition and chemical width of ultrathin amorphous films at grain boundaries in silicon nitride. *J Mater Res*. 1998;13:376-387.
37. Perdew JP. Accurate density functional for the energy: real-space cutoff of the gradient expansion for the exchange hole. *Phys Rev Lett*. 1985;55:1665.
38. Perdew JP, Burke K, Ernzerhof M. Generalized gradient approximation made simple. *Phys Rev Lett*. 1996;77:3865.
39. Aryal S, Sakidja R, Barsoum MW, Ching WY. A genomic approach to the stability, elastic, and electronic properties of the max phases. *Phys Status Solidi B* 2014;251:1480-1497.
40. Dharmawardhana C, Misra A, Ching W-Y. Quantum mechanical metric for internal cohesion in cement crystals. *Sci Rep*. 2014;4:1-8.
41. Aryal S, Sakidja R, Ouyang L, Ching W-Y. Elastic and electronic properties of ti 2 al (c x n 1− x) solid solutions. *J Eur Ceramic Soc*. 2015;35:3219-3227.
42. Aryal S, Matsunaga K, Ching W-Y. Ab initio simulation of elastic and mechanical properties of zn-and mg-doped hydroxyapatite (hap). *J Mech Behav Biomed Mater*. 2015;47:135-146.
43. Adhikari P, Dharmawardhana CC, Ching WY. Structure and properties of hydrogrossular mineral series. *J Am Ceram Soc*. 2017;100:4317-4330.
44. Li N, Ching W-Y. Structural, electronic and optical properties of a large random network model of amorphous sio 2 glass. *J Non-Cryst Solids*. 2014;383:28-32.
45. Walker B, Dharmawardhana CC, Dari N, Rulis P, Ching W-Y. Electronic structure and optical properties of amorphous geo 2 in comparison to amorphous sio 2. *J Non-Cryst Solids*. 2015;428:176-183.
46. Adhikari P, Xiong M, Li N, Zhao X, Rulis P, Ching W-Y. Structure and electronic properties of a continuous random network model of an amorphous zeolitic imidazolate framework (a-zif). *J Phys Chem C*. 2016;120:15362-15368.
47. Hunca B, Dharmawardhana C, Sakidja R, Ching W-Y. Ab initio calculations of thermomechanical properties and electronic structure of vitreloy $Zr_{41.2}$ $Ti_{13.8}$ $Cu_{12.5}$ Ni_{10} $Be_{22.5}$. *Phys Rev B*. 2016;94:144207-144210.

48. Baral K, Ching W-Y. Electronic structures and physical properties of na2o doped silicate glass. *J Appl Phys*. 2017;121:245103-245112.
49. Poudel L, Wen AM, French RH, et al. Electronic structure and partial charge distribution of doxorubicin in different molecular environments. *ChemPhysChem*. 2015;16:1451-1460.
50. Eifler J, Podgornik R, Steinmetz NF, French RH, Parsegian VA, Ching WY. Charge distribution and hydrogen bonding of a collagen α2-chain in vacuum, hydrated, neutral, and charged structural models. *Int J Quantum Chem*. 2016;116:681-691.
51. Poudel L, Steinmetz NF, French RH, Parsegian VA, Podgornik R, Ching W-Y. Implication of the solvent effect, metal ions and topology in the electronic structure and hydrogen bonding of human telomeric g-quadruplex DNA. *Phys Chem Chem Phys*. 2016;18:21573-21585.
52. Poudel L, Podgornik R, Ching W-Y. The hydration effect and selectivity of alkali-metal ions on polyethylene glycol (peg) models in cyclic and linear topology. *J Phys Chem A*. 2017;121:4721-4731.
53. Poudel L, Twarock R, Steinmetz NF, Podgornik R, Ching W-Y. Impact of hydrogen bonding in binding site between capsid protein and ms2 bacteriophage ssrna. *J Phys Chem B*. 2017;121:6321-6330.
54. Mulliken RS. Electronic population analysis on lcao–mo molecular wave functions. I. *J Chem Phys*. 1955;23:1833-1840.
55. Mulliken R. Electronic population analysis on lcao–mo molecular wave functions. Ii. Overlap populations, bond orders, and covalent bond energies. *J Chem Phys*. 1955;23:1841-1846.
56. Xu Y-N, Ching W. Electronic structure and optical properties of α and β phases of silicon nitride, silicon oxynitride, and with comparison to silicon dioxide. *Physi Rev B*. 1995;51:17379.
57. Zhang Y, Lee T-S, Yang W. A pseudobond approach to combining quantum mechanical and molecular mechanical methods. *J Chem Phys*. 1999;110:46-54.
58. Gu H, Cannon RM, Seifert HJ, Hoffmann MJ, Tanaka I. Solubility of si3n4 in liquid sio2. *J Am Ceram Soc*. 2002;85:25-32.
59. Tanaka I, Pezzotti G, Okamoto T, Miyamoto Y, Koizumi M. Hot isostatic press sintering and properties of silicon nitride without additives. *J Am Ceram Soc*. 1989;72:1656-1660.
60. Ii S, Iwamoto C, Matsunaga K, Yamamoto T, Yoshiya M, Ikuhara Y. Direct observation of intergranular cracks in sintered silicon nitride. *Philos Mag*. 2004;84:2767-2775.
61. Ii S, Iwamoto C, Matsunaga K, Yamamoto T, Ikuhara Y. Identification of crack path of inter-and transgranular fractures in sintered silicon nitride by in situ tem. *J Electron Microsc*. 2004;53:121-127.
62. Shibata N, Findlay S, Azuma S, Mizoguchi T, Yamamoto T, Ikuhara Y. Atomic-scale imaging of individual dopant atoms in a buried interface. *Nat Mater*. 2009;8:654-658.
63. Buban J, Matsunaga K, Chen J, et al. Grain boundary strengthening in alumina by rare earth impurities. *Science*. 2006;311:212-215.
64. Poudel L, Tamerler C, Misra A, Ching W-Y. Atomic-scale quantification of interfacial binding between peptides and inorganic crystals: the case of calcium carbonate binding peptide on aragonite. *J Phys Chem C*. 2017;121:28354-28363.
65. Chen M, Inoue A, Zhang W, Sakurai T. Extraordinary plasticity of ductile bulk metallic glasses. *Phys Rev Lett*. 2006;96:245502-245504.

AUTHOR BIOGRAPHIES

Wai-Yim Ching is a Curators' Distinguished Professor of Physics at the University of Missouri-Kansas City in USA. He leads the Electronic Structure Group (ESG) in the Department of Physics and Astronomy. He received BSc degree from University of Hong Kong in 2019 and Ph. D. degree in condensed matter physics at the Louisiana State University in 1974. He was a research associate at the University of Wisconsin-Madison from 1974-78 before joining UMKC as an Assistant Professor. His research focuses on condensed matter theory and computational materials science using first-principles methods. He developed the orthogonalized linear combination of atomic orbitals (OLCAO) method particularly suitable for large complex systems including biomolecular systems. With more than 40 years of experience, he is an author or co-author of over 425 journal articles with Google Scholar H-factor 68. He is an Academician of World Ceramic Academy (Advisory Board member: 2018-2022), Fellow of the American Ceramic Society, Fellow of the American Physical Society and Fellow of the Royal Society of Chemistry in Britain. He received the University of Missouri's Presidential Award for Sustained Career Excellence in 2017. He is an Associate Editor of the Journal of the American Ceramic Society and is on the Editorial Board of Nature Scientific Reports. He is currently supervising six Ph.D students.

Masato Yoshiya is Associate Professor in the Department of Adaptive Machine Systems, Osaka University, Japan. Trained as a metallurgist and metal physicist, he received his B.E., M.E, and Ph.D. from Kyoto University, Japan, based on his studies on theoretical calculations of ELNES and XANES based on *ab initio* calculations, its application to intergranular glassy films (IGF) of silicon nitride ceramics, and theoretical analyses to unveil mechanisms behind formation of the IGF by means of various computational techniques. In 2000, he joined Materials Science Division of Lawrence Berkeley National Laboratory as a visiting scholar while he is a JSPS fellow until the end of 2001

under supervisions of Drs. Rowland M. Cannon, Antoni Tomsia, and Robert O. Ritchie. Since 2002, he joined Japan Fine Ceramics Center (JFCC) primarily working on theoretical calculations to analyze thermal conduction in high temperature refractory materials including thermal barrier coatings for gas turbine blades, before joining Osaka University where he extended his computational studies to microstructure evolution including phase transformation and nucleation, gran boundary segregation of point defects and its impact on ionic conduction, thermoelectric ceramic materials, and thermodynamics and other properties of environmental barrier coatings. He is author or coauthor of 100 papers, an invited speaker in 12 symposia and an organizing committee member of 3 symposia directly organized or co-organized by The American Ceramic Societies in addition to more in other international conferences. 229words (150-250)

Puja Adhikari is Interdisciplinary Ph.D. student at University of Missouri-Kansas City working under supervision of Professor Wai-Yim Ching. She completed her M.S. degree in 2015 from UMKC. Her research area focuses on the study of electronic structure, mechanical and phonon properties of materials. She has worked on different kinds of materials such as pyrophosphates, glasses, clay and bio-molecules. She has so far authored or co-authored nine papers.

Paul Rulis is an Associate Professor of Physics at the University of Missouri – Kansas City (UMKC). He obtained a B.S. in Computer Science from Virginia Polytechnic Institute and State University in 1998 and a Ph.D. in Physics from UMKC in 2005. His broad interests lay in the development and application of computational condensed matter simulation programs so as to model the atomic and electronic structures of defective, nanostructured, and/or amorphous materials. Specifically, he leads the development of the orthogonalized linear combination of atomic orbitals (OLCAO) method for *ab initio* calculation of the electronic structure of solids. Current activities include the development of methods to support the Materials Genome Initiative and the application of a material-by-design method for the creation of novel amorphous molecular solids and pre-ceramic polymers. His research work has led him to author or co-author more than 60 journal articles. Outside of research and university teaching, he is an enthusiastic supporter of entrepreneurship and efforts to bring science, technology, engineering, arts, and mathematics into the lives of young students.

Yuichi Ikuhara is Professor and Director of Nanotechnology Center, Institute of Engineering Innovation at University of Tokyo since 2003. He received Dr.Eng. from Department of Materials Sciences, Kyushu University in 1988. He then has worked at Japan Fine Ceramics Center (JFCC) and Case Western Reserve University before joining UT. His current research interest is in interface and grain boundary phenomena, advanced transmission electron microscopy (STEM, HREM, EDS, EELS), high-temperature ceramics, dislocation technology, phase transformation, theoretical calculations and so on. Dr.Ikuhara is author and coauthor of about 720 scientific original papers in this field, and has more than 360 invited talks at international and domestic conferences. He received "Medal with Purple Ribbon"from the Emperor of Japan (2016), "Humboldt Research Award"from Alexander von Humboldt Foundation (2010), "Sosman Lecture Award" (2015) and "Ross Coffin Purdy Award" (2008) from the American Ceramics Society and so on. He is a fellow of the American Ceramics Society (2011), member of World Ceramic Academy (2014). He holds a group leader position at JFCC and WPI (World Premier International Research Center Initiative) professor at Tohoku University concurrently.

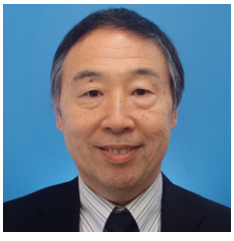

Isao Tanaka is Professor in the Department of Materials Science and Engineering, Kyoto University, Japan. Trained as a metal physicist, he received his B.E. and M.E. from Kyoto University and his Ph.D. from Osaka University. In 1987, he joined ISIR, Osaka University, as an assistant professor where he studied processing and characterization of high purity silicon nitride. He got an Alexander von Humboldt Fellowship in 1992 and stayed a year in Manfred Rühle's research group of Max Planck Institute for Metals Research in Stuttgart, Germany,

where he studied intergranular glassy films of silicon nitride ceramics. He returned to Kyoto University in 1993 and started to use quantum mechanical calculations and combined them with experimental techniques such as ELNES and XANES to study fundamental issues in a wide range of ceramic materials. He also studied electronic processes of defects, impurities, grain boundaries, surfaces, and their roles in macroscopic properties. In 2000s he made pioneering studies on theoretical calculation of thermo-physical properties of ceramic materials through first principles phonon calculations. Recently he is actively working on data-centric or informatics approach for discovery of new materials. Materials of his current interests are quite diverse including solid-state ionics, battery materials, oxide/nitride semiconductors, engineering ceramics, etc. He is author or coauthor of 400 papers. Recently he edited a book titled Nanoinformatics (Springer). He is a Fellow of American Ceramics Society and an associate editor of the Journal of American Ceramics Society. 235words (150-250)

How to cite this article: Ching W-Y, Yoshiya M, Adhikari P, Rulis P, Ikuhara Y, Tanaka I. First-principles study in an inter-granular glassy film model of silicon nitride. *J Am Ceram Soc*. 2018;101:2673–2688. https://doi.org/10.1111/jace.15538